Journal of Magnetic Resonance **139,** 165–174 (1999)
Article ID jmre.1999.1763, available online at http://www.idealibrary.com on IDEAL®

Electron Spin Lattice Relaxation Rates for S = ½ Molecular Species in Glassy Matrices or Magnetically Dilute Solids at Temperatures between 10 and 300 K

Yi Zhou, Bruce E. Bowler, Gareth R. Eaton, and Sandra S. Eaton

Department of Chemistry and Biochemistry, University of Denver, Denver, Colorado 80208

Received December 30, 1998; revised March 12, 1999

The temperature dependence of X-band electron spin–lattice relaxation between about 10 and 300 K in magnetically dilute solids and up to the softening temperature in glassy solvents was analyzed for three organic radicals and 14 S = ½ transition metal complexes. Contributions from the direct, Raman, local vibrational mode, thermally activated, and Orbach processes were considered. For most samples it was necessary to include more than one process to fit the experimental data. Debye temperatures were between 50 and 135 K. For small molecules the Debye temperature required to fit the relaxation data was higher in 1:1 water:glycerol than in organic solvents. For larger molecules the Debye temperature was less dependent upon solvent and more dependent upon the characteristics of the molecule. The coefficients of the Raman process increased with increasing *g* anisotropy and decreasing rigidity of the molecule. For the transition metal complexes the data are consistent with major contributions from local modes with energies in the range of 185 to 350 K (130 to 240 cm^{-1}). The coefficient for this contribution increases in the order 3*d* < 4*d* transition metal. For C_{60}^- anions there is a major contribution from a thermally activated process with an activation energy of about 240 cm^{-1}. For low-spin hemes the dominant contribution at higher temperatures is from a local mode or thermally activated process with a characteristic energy of about 175 cm^{-1}.

Key Words: **Debye temperature; electron spin–lattice relaxation; local vibrational mode; Orbach process; Raman process; thermally activated process; transition metal.**

INTRODUCTION

Electron spin relaxation rates reflect electronic structures of paramagnetic species and the dynamics of these species and their environment. Quantitative measures of electron spin relaxation rates as a function of temperature for transition metals in molecular complexes and for organic radicals are required to interpret the effect of a more rapidly relaxing spin on the relaxation rate for a more slowly relaxing spin and thereby determine the distance between the two paramagnetic centers (*1, 2*). Thus, we seek to understand the relaxation processes that occur for molecular species in doped solids and in glassy solvents at temperatures between about 10 K and the softening temperature of the glass.

Much of the classical work on electron spin–lattice relaxation processes was performed on ions in ionic lattices and at temperatures below about 20 K (*3, 4*). We are aware of only a few cases in which processes have been characterized over a wider temperature range. Castle and Feldman (*5, 6*) analyzed relaxation rates for the E' defect in crystalline and vitreous quartz between 4.2 and about 250 K in terms of the direct process and two local modes. The relaxation for atomic hydrogen in fused silica between 2 and 100 K could be modeled with either an Orbach process or a local mode (*7*). The data for atomic hydrogen in fused silica demonstrate that the similarity in temperature dependence predicted by some relaxation processes within limited temperature intervals requires that assignments be based not only on the temperature dependence of the relaxation rates, but also on the plausibility of the parameters obtained by fitting to various models. Hoffmann *et al.* (*8*) analyzed spin–lattice relaxation for Cu(II) in triglycine selenate between 4.2 and 90 K in terms of the direct process and the Raman process with a Debye temperature of 168 K. Gayda *et al.* (*9*) studied spin–lattice relaxation for a 2-iron–2-sulfur protein between 1.25 and 130 K. To fit the data several processes were required: below 3 K a phonon bottleneck, between about 3 and 30 K the Raman process, and near 100 K an Orbach process. Since the predicted temperature dependence of spin lattice relaxation ($1/T_1$) is the same for the Orbach and local mode processes in the temperature range for which data were available, assignment of the relaxation processes required information beyond the EPR studies (*10*). These limited examples suggest that more than one relaxation process may be required to fit the temperature dependence of electron spin–lattice relaxation between 10 K and the softening point of a glass.

It has been proposed that modulation of nuclear hyperfine splitting contributes to electron $1/T_1$ (*11*). However, the following observations have been made for magnetically dilute S = ½ species in the temperature range of about 30 to 150 K. For nitroxyl radicals in glassy solutions, $1/T_1$ is the same within experimental uncertainty for natural abundance and ^{15}N-enriched samples (*12*). For a chromium(V) complex in 1:1

1090-7807/99 $30.00

water:glycerol at 100 K, $1/T_1$ is similar for natural abundance Cr (predominantly I = 0) and for isotopically enriched ^{53}Cr ($I = \frac{3}{2}$) and $1/T_1$ is independent of m_I (*13*). For a Mo(V) porphyrin, $1/T_1$ is approximately the same for isotopes with I = 0 and $I = \frac{5}{2}$ (*14*). For single crystals of bis(diethyldithiocarbamato)Cu(II), $Cu(dtc)_2$, doped into $Ni(dtc)_2$ (*15*), or for (tetraphenylporphyrinato)Cu(II), CuTPP, doped into ZnTPP (*16*), $1/T_1$ is independent of copper m_I. The similarity of values of $1/T_1$ for metal isotopes with and without nuclear spins and the absence of dependence on m_I indicate that for this range of species, modulation of nuclear hyperfine splitting is not the dominant contribution to $1/T_1$.

It seems likely that the dominant contributions to spin–lattice relaxation for $S = \frac{1}{2}$ species are due to modulation of spin–orbit coupling (*16*). Numerical calculation of the matrix elements that describe the modulation of spin–orbit coupling by various relaxation processes is difficult. The alternate approach taken here is to fit the experimental relaxation data for a series of well-characterized molecular species and to examine the fit parameters for various relaxation processes. The analysis includes data sets for 3 organic radicals and 14 transition metal complexes.

EXPERIMENTAL METHODS

Tempone (2,2,6,6-tetramethylpiperidin-1-oxyl, Aldrich Chemical Company, Milwaukee, WI) and horse heart myoglobin (Sigma, St. Louis, MO) were used without purification. The Nycomed symmetric-trityl radical (*17, 18*) was a gift from Prof. Howard Halpern, University of Chicago. Mutants of sperm whale myoglobin in which valine 66 was replaced by cysteine (Mb-V66C) or lysine 98 was replaced by cysteine (Mb-K87C) (*19*) were expressed in bacteria as described by Springer and Sliger (*20*). The genetically engineered sperm whale myoglobins have an additional methionine at the N-terminus that is not present in the naturally occurring protein, but this modification does not affect the protein structure (*21*). A nitroxyl spin label was attached to the cysteines in Mb-V66C and Mb-K98C and the heme iron was oxidized to Fe(III) to prepare R-Mb-V66C and R-Mb-K98C, respectively (*19*). Cyanide or imidazole was added to the samples to make low-spin Fe(III) adducts. Saturation recovery measurements of $1/T_1$ were performed using the procedures described in the following paragraphs. In addition, previously published data for the temperature dependence of $1/T_1$ was analyzed for tempone in 1:1 water:glycerol (*12, 22*); C_{60} anions (*23*); the vanadyl complex of 5-(4-carboxyphenyl)-10,15,20-tri(tolyl)porphyrin, VOTTP-COOH (*16*); the vanadyl complex of 5,10,15-tri-*p*-tolyl-20-(4′-(4-methyl)bipyridyl)porphyrin, VOTTP-bipy (*24*); VO^{2+}(aq) in 1:1 water:glycerol (*25*); chromyl bis(2-ethyl-2-hydroxybutyrate), $CrO(HEBA)_2^-$ (*22*); the nitrido chromium(V) complex of 5,10,15,20-tetratolylporphyrin, CrNTPP (*26*); $Cu(dtc)_2$ (*15*); CuTTP (*16*); the bis(hexafluoroacetylacetonato)Cu(II) adduct of ZnTTPbipy, ZnTTPbipy-$Cu(hfac)_2$ (*24*); bis(hexafluoroacetylacetonato)(4,4′-dimethyl-2,2′-bipyridyl)Cu(II), $Cu(hfac)_2(Me_2\text{-bipy})$ (*24*); low-spin (5,10,15,20-tetraphenylporphyin)bis(1-methylimidazolate)iron(III), $FeTPP(Im)_2^+$ (*27*); (5,10,15,20-tetratolylporphyrin) oxomolybdenum(V) ethoxide, MoOTTP(OEt) (*14*); and silver(II) complex of (5,10,15,20-tetratolylporphyrin), AgTTP (*16*). The solvents and solvent mixtures used in these studies form glasses at low temperatures. Sample concentrations were 0.5 to 1.5 mM. Measurements at 90 to 130 K indicate that the relaxation rates for these compounds are not significantly concentration dependent under these conditions.

Spin–lattice relaxation rates, $1/T_1$, up to about 10^6 s^{-1} were measured by long-pulse saturation recovery on a locally constructed X-band spectrometer (*28*). Temperatures between 10 and 60 K were obtained with an Oxford ESR900 flow cryostat. Temperatures between 90 and 140 K were obtained with a Varian liquid-nitrogen-cooled gas flow system. The temperature at the sample as a function of variable temperature controller readout was calibrated by replacing the sample with a tube containing a thermocouple immersed in 1:1 H_2O:glycerol. Between 10 and 60 K the temperature at the sample is strongly dependent upon the helium flow rate, which causes as much as 2 K uncertainty in temperature. Between 90 and 140 K the uncertainty in temperature is less than 1 K. The effects of spectral diffusion were monitored by measuring the saturation recovery time constant as a function of the length of the saturating pulse. The data described in this paper were obtained in the limit where the saturation recovery time constant is independent of the length of the pump pulse. Typically, the length of the pump pulse was greater than the saturation recovery time constant. Experimental data were fitted to a single exponential using a nonlinear least-squares algorithm. The fit to a single exponential typically was good. Deviation from a single exponential may be due to a distribution in relaxation rates.

For C_{60} anions, $FeTPP(Im)_2^+$, R-Mb-Im, and R-Mb-CN, the linewidths of the EPR signals in the CW spectra are temperature dependent above about 40 to 60 K. In this temperature range the electron spin T_2 was determined from the temperature-dependent contribution to the linewidth (*23, 19*) and the assumption was made that $T_1 = T_2$.

By minimizing the sum of the residuals on a log–log scale, the temperature dependence of $1/T_1$ was fitted to

$$\frac{1}{T_1} = A_{\mathrm{dir}}T + A_{\mathrm{Ram}}\left(\frac{T}{\theta_{\mathrm{D}}}\right)J_8\left(\frac{\theta_{\mathrm{D}}}{T}\right) + A_{\mathrm{loc}}\left[\frac{e^{\Delta_{\mathrm{loc}}/T}}{(e^{\Delta_{\mathrm{loc}}/T}-1)^2}\right] + A_{\mathrm{Orb}}\left[\frac{\Delta_{\mathrm{Orb}}^3}{e^{\Delta_{\mathrm{Orb}}/T}-1}\right] + A_{\mathrm{therm}}\left[\frac{2\tau_{\mathrm{c}}}{1+\omega^2\tau_{\mathrm{c}}^2}\right], \qquad [1]$$

where T is temperature in kelvins, A_{dir} is the coefficient for the contribution from the direct process, A_{Ram} is the coefficient for the contribution from the Raman process, θ_{D} is the Debye temperature, J_8 is the transport integral,

$$J_8\left(\frac{\theta_D}{T}\right) = \int_0^{\theta_D/T} x^8 \frac{e^x}{(e^x - 1)^2}\, dx,$$

A_{loc} is the coefficient for the contribution from a local vibrational mode, Δ_{loc} is the energy for the local mode in kelvins, A_{Orb} is the coefficient for the contribution from the Orbach process, Δ_{Orb} is the energy separation between the ground state and the excited state for the Orbach process, A_{therm} is the coefficient for the contribution from the thermally activated process, τ_C is the correlation time for the thermally activated process $= \tau_c^o e^{E_a/T}$, E_a is the activation energy for the thermally activated process, and τ_c^o is the preexponential factor.

Mathematical expressions for the temperature dependence of spin–lattice relaxation are taken from the following references: Raman process (*29, 30*), local mode (*5*), Orbach process (*31*), and thermally activated process (*32*).

Strategy Used in Fitting the Experimental Data

The temperature dependence of $1/T_1$ for the Raman process is distinctive if data are available over a sufficiently wide temperature range. The data for most of the samples studied here included a temperature region in which the Raman process dominated. This process was used as the first component when fitting the experimental data. Additional contributions were then added as required to fit the data. The weak temperature dependence of relaxation produced by the direct process is distinctive, and its effects were detectable primarily at temperatures below about 10 K. Over a limited temperature interval ($T < \Delta_{loc}$, Δ_{Orb}, or E_a), the temperature dependence of $1/T_1$ due to a local mode, an Orbach process, or a thermally activated process is similar, and distinctions between these processes require knowledge of the electronic and vibrational structure of the paramagnetic species. For example, there are no known low-lying electronic excited states for nitroxyl radicals or for the distorted octahedral or square pyramidal d^1 or d^9 transition metal complexes included in this study, so an Orbach process was not considered for these systems. Low-lying excited states are known to exist for low-spin Fe(III), so an Orbach process was considered. The distinction between a local mode and a thermally activated process relates to the rate and amplitude of the proposed perturbation (*32*). The thermally activated model is valid for short correlation times and greater anharmonicity than fit the assumptions of the Raman and local mode models. This distinction suggests that at higher temperatures the thermally activated model is more likely to be applicable than a local mode. Therefore, the fit parameters for the highest temperature processes given in Table 1 are based on assignment as a thermal process.

For each sample, the temperature dependence of $1/T_1$ was fitted with the smallest number of contributing processes consistent with the experimental data. The resulting best-fit parameters are given in Table 1. Based on the residuals from the fitting procedure the uncertainty in the Debye temperature or in the characteristic energy for a process (Δ_{loc}, Δ_{Orb}, or E_a) is about 10% for the dominant contribution to the relaxation rate. Errors in the Debye temperature (or in the characteristic energy for other processes) and the coefficient for that process are correlated. For example, changing the value of θ_D from 105 to 110 K requires increasing A_{Ram} by about 15% to give approximately the same relaxation rates. In addition, uncertainties in temperature, particularly at low temperature, could be a source of larger systematic errors. Uncertainties in fitted parameters are substantially larger for processes that make only a small contribution to the experimental relaxation rate in the temperature range examined.

RESULTS

The temperature dependence of $1/T_1$ for the Nycomed symmetrical-trityl radical (*18*) in 1:1 water:glycerol is shown in Fig. 1. Over the temperature range from 22 to about 100 K the data could be fitted to a Raman process with $\theta_D = 105$ K (Table 1). Above about 100 K the relaxation rate increases faster with increasing temperature than is predicted by the Raman process alone (Fig. 1). The highest-temperature data point (198 K) is close to the softening point of the water:glycerol glass. The additional contribution could be modeled as a thermally activated process or as a local mode, and a distinction between the two processes cannot be made based on data within the available temperature range. The data for trityl radical in 9:1 *n*-propanol:methanol are similar to the data in 1:1 water:glycerol and could be modeled with a decrease of the Debye temperature to 80 K and a small decrease in A_{Ram} (Table 1).

The relaxation rates for the nitroxyl radical tempone in 1:1 water:glycerol are shown in Fig. 1. Between about 20 and 80 K the data could be fitted to a Raman process with $\theta_D = 112$ K. At higher temperatures an additional process, either thermal or local mode, contributes to the relaxation. As noted previously, spin–lattice relaxation rates for nitroxyl radicals at 100 K are substantially faster in solvents such as decalin or sucrose octaacetate than in more strongly hydrogen bonding solvents such as 1:1 water:glycerol (*12*). Fitting of the temperature dependence of $1/T_1$ for tempone gave substantially smaller values of θ_D in decalin, sucrose octaacetate, or 9:1 *n*-propanol:methanol than in 1:1 water:glycerol (Table 1), which suggests that changes in the Debye temperature are a major factor in the solvent dependence of relaxation rates observed previously at 100 K. In both decalin and 9:1 *n*-propanol:methanol, the Raman process accounted for the temperature dependence of $1/T_1$ over the full temperature range examined, which extended up to 124 or 130 K, respectively. Because of the low softening temperatures of decalin and 9:1 *n*-propanol:methanol glasses, data for tempone in these solvents were not obtained at the higher temperatures for which the additional contribution to

TABLE 1
Contributions to Spin–Lattice Relaxation Determined by Fitting to Eq. [1]

Sample	Lattice	Temperature range (K)	g values[a]	Direct A_{dir}	Raman A_{Ram}, θ_D	Local A_{loc}, Δ_{loc}[b]	Thermal A_{therm}, E_a[b], τ_c^o
Organic radicals							
Trityl	H_2O:glycerol	22–173	2.005		5.3×10^3, 105		5.4×10^{15}, 1050, 5.5×10^{-12} [c]
Trityl	9:1 *n*-PrOH:MeOH	12–132	2.005		3.4×10^3, 80		
Tempone	H_2O:glycerol	14–200	2.009, 2.005, 2.002		4.2×10^4, 112		2.9×10^{15}, 600, 5.5×10^{-12} [c]
Tempone	decalin	10–130	2.009, 2.005, 2.002		3.9×10^4, 67		
Tempone	sucrose octaacetate	11–300	2.009, 2.005, 2.002		2.3×10^4, 51		6.1×10^{16}, 1150, 4.5×10^{-12}
Tempone	9:1 *n*-PrOH:MeOH	12–124	2.009, 2.005, 2.002		2.4×10^4, 54		
C_{60}^-	MeTHF	10–298	1.995, 2.000		6.0×10^7, 95		6.8×10^{19}, 330, 3.3×10^{-12}
C_{60}^-	toluene:acetonitrile	9–217	1.994, 1.999		1.6×10^7, 75		3.3×10^{19}, 370, 3.9×10^{-12}
C_{60}^{3-}	DMSO	6–134	2.008, 2.000, 1.995		1.3×10^7, 50		2.6×10^{19}, 334, 3.1×10^{-12}
3*d* transition metals							
VOTTP-COOH	ZnTTP solid	41–260	1.984, 1.964	11.5	6.0×10^4, 100	4.0×10^5, 350	5.5×10^{16}, 950, 6.5×10^{-12} [c,d]
VOTTP-bipy	toluene:$CHCl_3$	17–120	1.984, 1.966	8.5	6.5×10^4, 100	6.5×10^5, 350	
VO^{2+} (aq)	H_2O:glycerol	11–100	1.980, 1.937		7.4×10^5, 120	7.9×10^5, 185	
$CrO(HEBA)_2^-$	H_2O:glycerol	10–150	1.971 1.972 1.983	1.3	1.3×10^5, 115	8.7×10^5, 370	
CrNTPP	tol:THF	18–130	1.994, 1.956	4.8	1.2×10^5, 135	4.3×10^5, 320	8.0×10^{16}, 750, 6.5×10^{-12} [c]
$Cu(dtc)_2$	$Ni(dtc)_2$ solid	26–298	2.018, 2.083	30	5.8×10^5, 90	5.7×10^5, 240	
$Cu(dtc)_2$	toluene:$CHCl_3$	25–140	2.019, 2.087	20	3.8×10^5, 65		2.5×10^{17}, 650, 5.5×10^{-12}
CuTTP	ZnTTP solid	30–200	2.045, 2.190	19.5	4.8×10^5, 120	1.5×10^6, 250	9.7×10^{17}, 950, 5.5×10^{-12}
CuTTP	toluene:$CHCl_3$	20–135	2.049, 2.203	14.5	5.5×10^5, 110	3.4×10^5, 250	8.6×10^{17}, 650, 5.5×10^{-12}
ZnTTPbipy-$Cu(hfac)_2$	toluene:$CHCl_3$	15–100	2.063, 2.288		1.2×10^7, 125[e]		
$Cu(hfac)_2$-(Me_2-bipy)	toluene:$CHCl_3$	10–50	2.075, 2.277		6.0×10^6, 70[e]		
$FeTPP(Im)_2^+$	toluene:$CHCl_3$	11–130	1.50, 2.13, 2.61		1.2×10^7, 80		0.8×10^{20}, 240, 5.5×10^{-12} [f]
R-Mb-Im	H_2O:glycerol	6–138	1.44, 2.22 3.02	20	1.2×10^8, 82		3.0×10^{20}, 265, 6.5×10^{-12} [f]
R-Mb-CN	H_2O:glycerol	5–60	~1., 1.72, 3.48	28	9.0×10^8, 78		4.5×10^{21}, 275, 6.5×10^{-12} [f]
4*d* transition metals							
MoOTTP-OEt	toluene:$CHCl_3$	20–140	1.967, 1.971		1.8×10^5, 120[g]	3.6×10^6, 350	1.9×10^{18}, 750, 6.5×10^{-12}
AgTTP	H_2TTP, solid	28–115	2.040, 2.110		1.3×10^5, 120[g]	1.1×10^7, 270	
AgTTP	toluene:$CHCl_3$	28–114	"			1.3×10^7, 275	

[a] For complexes with axial symmetry g values are given in the order $g_\perp$, $g_\parallel$.
[b] Energies in kelvins.
[c] Contribution from thermal process is small and has observable impact only at temperatures above about 130 K.
[d] Alternate fitting is with second local mode with $A = 5.5 \times 10^6$ and $\Delta_{loc} = 950$ K.
[e] Data can also be fit with a local mode instead of a Raman process.
[f] Comparable fit to the data also could be obtained with either an Orbach process or a local mode.
[g] Dominant contributions are from local mode and/or thermal process. There is substantial uncertainty in the parameters for the Raman process.

relaxation was observed in 1:1 water:glycerol or sucrose octaacetate.

The temperature dependence of the electron spin relaxation rate for C_{60}^{-1} in methyl-THF is shown in Fig. 2. The fit line is the sum of contributions from two processes. The low temperature process is assigned as Raman ($\theta_D = 90$ K) by analogy with the tempone and trityl radicals. For C_{60}^{-1} it was possible to obtain data at temperatures extending beyond the melting point of the solvent, which showed that the relaxation reached a plateau at higher temperatures. This temperature dependence is characteristic of a thermally activated process. Neither an Orbach process nor a local mode predicts a plateau in the relaxation rate. Similar temperature dependence of relaxation rates was observed for C_{60}^{-1} in methyl-THF (Fig. 2) or 2:1 toluene:acetonitrile and for C_{60}^{-3} in DMSO (Table 1).

Spin–lattice relaxation rates for two vanadyl complexes are shown in Fig. 3. For neither complex was it possible to fit the experimental temperature dependence with a single relaxation process. The temperature dependence of $1/T_1$ for VOTTP-bipy in 2:1 toluene:$CHCl_3$ (Fig. 3) and for VOTTP-COOH doped into ZnTPP (*16*) are similar and could be fitted with a combination of a direct process dominating at low temperature, the Raman process at intermediate temperatures and a local mode at higher temperatures (Table 1, Fig. 3). To fit the data in the doped solid at higher temperatures (up to 260 K) than were examined for the glassy solution (up to 120 K) an additional process was required, which was modeled as thermally activated. An alternative assignment for this additional higher-temperature contribution would be a second local mode.

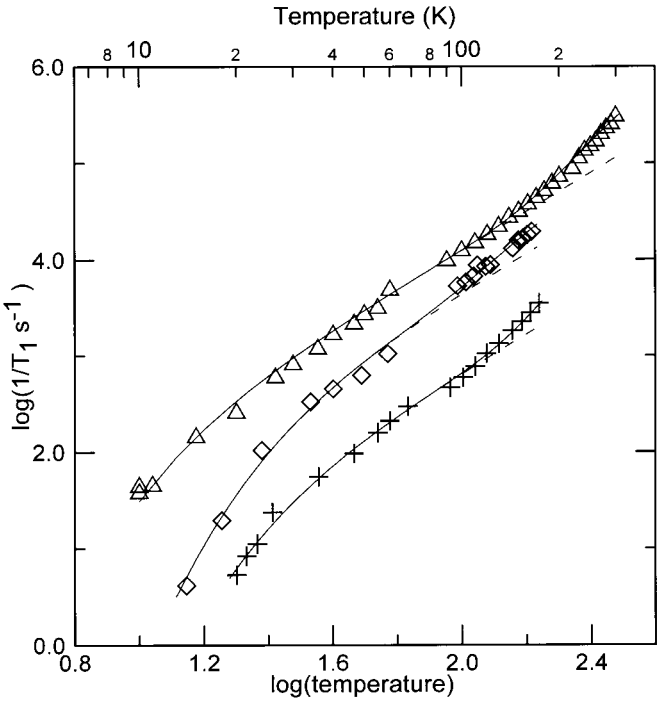

FIG. 1. Temperature dependence of X-band spin–lattice relaxation rates for 0.2 mM Nycomed symmetrical-trityl radical in 1:1 water:glycerol (+), 1 mM tempone in 1:1 water:glycerol (◇) (*22*), and 1 mM tempone in glassy sucrose octaacetate (△). The data for tempone were obtained in the center of the spectrum. The solid lines through the data are the fits obtained using Eq. [1] and the parameters in Table 1. The dashed lines are the curves calculated using only the Raman contribution to the relaxation rates.

Above about 20 K the relaxation rates for VO^{2+} (aq) in 1:1 water:glycerol were faster than for VOTTP-bipy or VOTTP-COOH (Fig. 3). The data for VO^{2+} were modeled with the Raman process and a local mode. The importance of a local mode, rather than a thermally activated process, as the second contribution to the relaxation is suggested for VO^{2+} because the impact of this mode was evident at temperatures above about 25 K, which is much lower than observed for other processes that were assigned as thermally activated. In addition, if the second contribution were modeled as a thermally activated process it would require an activation energy on the order of 180 K, which is substantially lower than observed for other processes that were assigned as thermally activated. The V═O stretching frequency is about 980 cm^{-1} (*33*), which is too high an energy to be the relevant mode. Faster relaxation for VO^{2+} than for the vanadyl porphyrins may occur because other local modes in the aquo complex are "softer" than the metalloporphyrins.

The spin–lattice relaxation rates and the temperature dependence of the rates for $CrO(HEBA)_2^-$ in 1:1 water:glycerol and for CrNTPP in 9:1 toluene:THF are similar to each other and similar to that for VOTTP-bipy and VOTTP-COOH, which also have a d^1 electron configuration. As noted previously (*34*), the relatively slow relaxation for Cr(V) in these distorted octahedral and square pyramidal complexes is the result of the high energy of the lowest electronic excited state. The data for the Cr(V) complexes were fitted to the sum of contributions from the direct process, the Raman process, and a local mode (Table 1). At the highest temperatures for which data were available for CrNTTP, there was a small additional contribution that was modeled as a thermally activated process.

For $Cu(dtc)_2$ doped into $Ni(dtc)_2$ the temperature dependence of the relaxation was modeled by the direct process (a minor contribution at the lowest temperatures), the Raman process, and a local mode (Fig. 4). In glassy 2:1 toluene:$CHCl_3$ solution the melting/softening temperature is below the temperature region in which the local mode made a significant contribution to the relaxation for the doped solid, so a local mode was not required to fit the data in the glass (Table 1). In the glass, an additional contribution was observed above about 100 K that was attributed to a thermally activated process. The relaxation rates for CuTTP in a doped solid or in glassy solution are similar to those for $Cu(dtc)_2$ and were modeled with the direct process (small contribution at the lowest temperatures), the Raman process, a local mode, and a thermally activated process (small contribution at the highest temperatures). In both $Cu(dtc)_2$ and CuTTP the d^9 Cu(II) is approximately square planar.

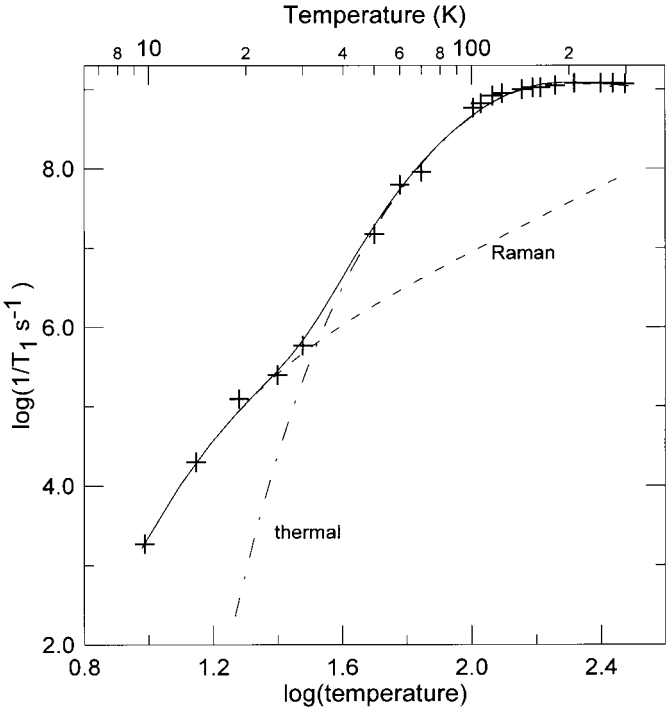

FIG. 2. Temperature dependence of X-band spin–lattice relaxation rates in the perpendicular plane for 0.3 mM C_{60}^- anion in methyl-THF (+) (*23*). The solid line through the data is the fit obtained using Eq. [1] and the parameters in Table 1. The contributions to the relaxation from the Raman process (– – –) and the thermally activated process (– · – · –) are shown separately.

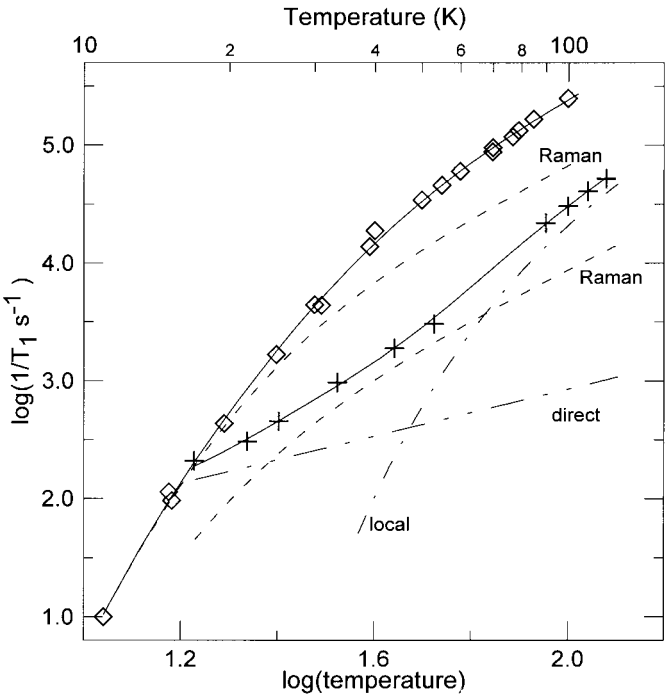

FIG. 3. Temperature dependence of X-band spin–lattice relaxation rates for 1 mM VOTPP-COOH in 2:1 toluene:$CHCl_3$ (+) (*16*) and for 1 mM VO^{2+} in 1:1 water:glycerol (◇) (*25*) for the $m_I = -\frac{1}{2}$ perpendicular transitions. The solid lines through the data are the fits obtained using Eq. [1] and the parameters in Table 1. The contributions from individual processes to the relaxation for VOTPP-COOH are direct (– · · – · · –), Raman (– – –), and local mode (– · – · –).

The relaxation rate for six-coordinate Cu(II) in $Cu(hfac)_2(Me_2\text{-bipy})$ is substantially faster than for square planar, four-coordinate $Cu(dtc)_2$, and the data between 10 and 50 K could be modeled with the Raman process (Fig. 4). However, the faster rate of relaxation for the six-coordinate complex is not due entirely to the change in coordination number. Between 10 and 50 K the relaxation rates for ZnTTPbipy-$Cu(hfac)_2$ are about an order of magnitude slower than for $Cu(hfac)_2(Me_2\text{-bipy})$ (*24*). In both complexes the Cu(II) is six-coordinate with N_2O_4 coordination and the *g*- and *A*-values are similar (Table 1, *24*). However, in ZnTTPbipy-$Cu(hfac)_2$ the bipyridyl is built into the porphyrin, which may substantially restrict the conformational flexibility of the complex compared with that of $Cu(hfac)_2(Me_2\text{-bipy})$. The relaxation data for ZnTTPbipy-$Cu(hfac)_2$ also could be modeled with the Raman process (Table 1).

It has been proposed that the spin–lattice relaxation rates for low-spin Fe(III) in heme proteins reflected the fractal dimension of the protein (*35*). However, we observed that the spin–lattice relaxation rates are very similar for low-spin Fe(III) in small-molecule porphyrin complexes and in methemoglobin (*36*), which suggests that a common explanation should be sought for the relaxation in protein and nonprotein environments. Spin–lattice relaxation rates for the low-spin heme iron in the methylimidazole adduct of R-MbV66C and R-MbK98C and for the cyanide adducts of horse heart myoglobin, R-Mb-V66C, and R-Mb-K98C are shown in Fig. 5. In the myoglobin variants the site of the mutation is distant from the heme pocket (*19*) and is not expected to affect the iron relaxation rate, which is consistent with the observation of similar relaxation rates for the two mutants and for horse heart myoglobin. The experimental data for both the imidazole and cyanide adducts were fitted with the direct process (small contribution at the lowest temperatures), the Raman process, and an additional process at higher temperatures (Fig. 5). Comparable fit to the experimental data could be obtained assuming that the higher temperature process was thermally activated, a local mode, or an Orbach process. Similarly, the data for $FeTPP(Im)_2^+$ could be fitted as the sum of the Raman process and a second process at higher temperatures (Table 1).

Data were analyzed for two 4*d* metalloporphyrin complexes, MoOTTP(OEt), $4d^1$, and AgTTP, $4d^9$. As noted previously (*16*), the temperature dependence of $1/T_1$ for these complexes is greater than for similar complexes with $3d^1$ or $3d^9$ electron configurations. To fit the data for the Mo(V) and Ag(II) porphyrins the Debye temperature was fixed at 120 K, which is the average of the values observed for the $3d^1$ and $3d^9$ porphyrin complexes (Table 1). The coefficient A_{Ram} and contributions

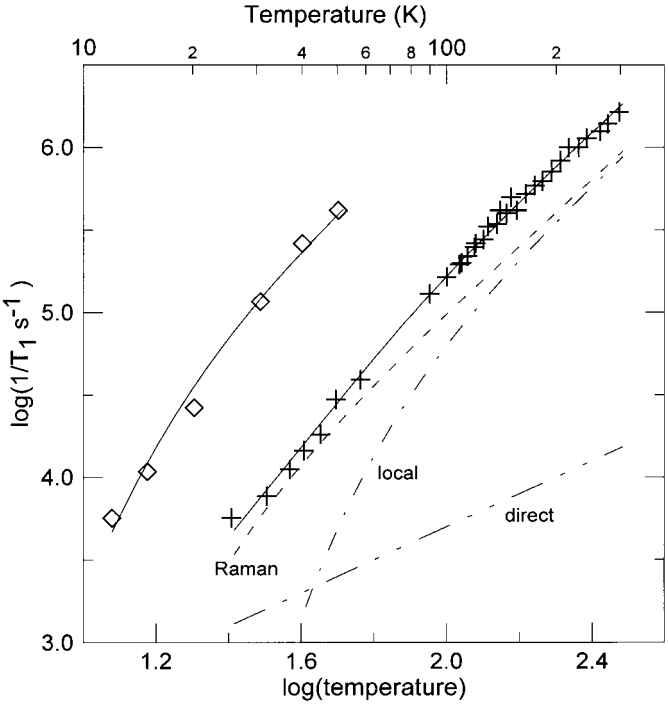

FIG. 4. Temperature dependence of X-band spin–lattice relaxation rates for ~0.2% $Cu(dtc)_2$ doped into solid $Ni(dtc)_2$ (+) (*15*) and for 1 mM $Cu(hfac)_2(Me_2\text{-bipy})$ in 2:1 toluene:$CHCl_3$ (◇) (*24*) for the $m_I = \frac{1}{2}$ perpendicular transitions. The solid lines through the data are the fits obtained using Eq. [1] and the parameters in Table 1. The contributions from individual processes to the relaxation for $Cu(dtc)_2$ are direct (– · · – · · –), Raman (– – –), and local mode (– · – · – ·).

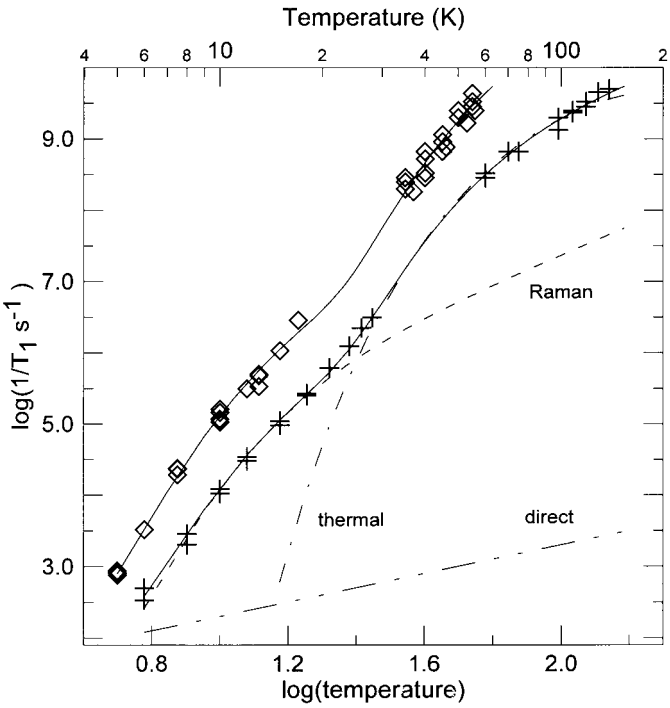

FIG. 5. Temperature dependence of X-band spin–lattice relaxation rates for 1 mM imidazole adducts R-Mb-V66C-Im and R-Mb-K98C-Im (+), and 1 mM cyanide adducts R-Mb-V66C-CN, R-Mb-K98C-CN, and horse heart myoglobin cyanide (◇) in 1:1 water:glycerol (*19*). The solid lines through the data are the fits obtained using Eq. [1] and the parameters in Table 1. The contributions from individual processes to the relaxation for the imidazole adducts are direct (– · · – · · –), Raman (– – –), and thermal mode (– · – · –).

from other processes were adjusted to obtain the best fit to the data. For MoOTTP(OEt) the predominant contribution is from a local mode and there is a smaller contribution at higher temperature that was modeled as thermally activated. For AgTTP in glassy solution or doped solid the predominant contribution is from a local mode. The temperature range for which data could be obtained for AgTTP (maximum of 115 K) may not extend to high enough temperatures to show the effects of thermally activated processes.

DISCUSSION

For $S = \frac{1}{2}$ samples with a range of molecular electronic structures the temperature dependence of $1/T_1$ was fitted to Eq. [1] and the best-fit parameters are summarized in Table 1. In each case the data were fitted to the minimum number of contributing processes consistent with the experimental data. In the following paragraphs we examine trends in the parameters.

Raman process. For the organic radicals trityl and tempone, the Raman process is the dominant contribution to the relaxation over most of the temperature range for which experimental data were obtained. The slopes of the plots in Fig. 1 above about 30 K are about 2, which is expected for the Raman process in the high-temperature limit (*37*). The onset of limiting behavior occurs at a smaller fraction of θ_D in glasses than in crystalline solids because of the greater role of lower frequency vibrations in glasses (*38, 39*). For the other species examined, there is a temperature range in which the relaxation is consistent with the Raman process, although substantial contributions from one or more additional processes are required to interpret the experimental data over the full temperature range.

For all of the samples studied the Debye temperature (θ_D) is between 50 and 135 K. These values are in a reasonable range, since the Debye temperature for polycrystalline ice is about 200 K (*40*) and lower values are expected for organic glasses because the vibrational modes are softer (*41*). Literature values of Debye temperatures for molecular species include 22 to 36 K for transition metal salts of lidocaine (*42*), about 33 K for a tin-containing liquid crystal (*43*), 46–57 K for 4-coordinate alkyl tin halides (*44*), 88 K for $[Eu(\eta^6\text{-}C_6Me_6)(AlCl_4)_2]_4$ (*45*), 88–100 K for one-dimensional organic conductors derived from TCNQ (*46*), about 100 K for glassy aqueous 1 M NaOH (*47*), 102–144 K for 6-coordinate alkyl tin halides (*48*), about 120 K for bis(ethylenedithio)tetrathiofulvene triiodide (*49*), and 128 K for $[(CF_3COO)_3EuHAl(C_2H_5)\cdot 2THF]_2$ (*50*).

In 1:1 water:glycerol the Debye temperatures for the relatively small molecules tempone (112 K), VO^{2+} (120 K), and $CrO(HEBA)_2^-$ (115 K) are similar. These Debye temperatures are higher than were observed for small molecules in organic solvents: tempone in decalin (67 K), tempone in 9:1 *n*-propanol:methanol (54 K), $Cu(dtc)_2$ in 2:1 toluene:$CHCl_3$ (65 K), and $Cu(hfac)_2(Me_2\text{-bipy})$ in 2:1 toluene:$CHCl_3$ (70 K). The difference in θ_D values between 9:1 *n*-propanol:methanol and 1:1 water:glycerol is smaller for the bulky trityl radical (80 K vs 105 K) than for tempone (54 K vs 112 K) (Table 1). The unpaired electron of the trityl radical is largely localized on the central carbon, which is insulated from solvent. The trityl molecule is sufficiently large (m.w. = 1151 g/mol) that θ_D is strongly influenced by the molecule itself, with some impact of the solvent. The tempone radical is much smaller and the unpaired electron is in close proximity to the solvent, which makes θ_D more solvent dependent. For the d^1 and d^9 metalloporphyrins θ_D is in the range of 110 to 135 K, independent of whether the host is a polycrystalline diamagnetic metalloporphyrin or glassy 2:1 toluene:$CHCl_3$. The small range in θ_D for the metalloporphyrins suggests that, analogous to trityl, the molecule largely defines the motions that contribute to the Raman process at the paramagnetic center. In contrast to these metalloporphyrins, the Debye temperatures for the low-spin Fe(III) porphyrins, whether small molecule or protein, are in the range of 78–82 K. These lower values suggest that the additional axial ligands in these complexes have a substantial impact on the motions that contribute to the Raman process. These Debye temperatures are somewhat higher than the θ_D = 60 K obtained for two iron–sulfur ferredoxins (*9, 10*). Debye

temperatures between 56 and 65 K were observed for alkyl tin derivatives of DNA (*51*).

The coefficients of the Raman contribution, A_{Ram}, are expected to depend on several factors. (1) As the rigidity of the paramagnetic center decreases, the paramagnetic center becomes more sensitive to motions of its surroundings and A_{Ram} is expected to increase. (2) As g anisotropy and deviation of g values from 2.0023 increase, the same amplitude of motion of surrounding atoms has a greater impact on the paramagnetic center and A_{Ram} is expected to increase. The g values reflect spin–orbit coupling so, equivalently, A_{Ram} is expected to increase as spin–orbit coupling increases. For example, A_{Ram} is greater for tempone (2.5×10^4 to 3.9×10^4) than for trityl radical ($\sim 4 \times 10^3$), consistent with the greater g anisotropy for tempone (Table 1). The substantially larger A_{Ram} for the C_{60} anions ($\sim 10^7$) than for tempone or trityl is attributed to a combination of greater spin–orbit coupling and to the wide variety of low-energy motions accessible to the buckyball. For the vanadyl and Cr(V) porphyrins A_{Ram} ($\sim 1 \times 10^5$) is smaller than for the Cu(II) porphyrins ($\sim 5 \times 10^5$), which is consistent with the larger g anisotropy for Cu(II) than for vanadyl or Cr(V) (Table 1). A_{Ram} is larger for the six-coordinate $Cu(hfac)_2bipy_2$ adducts ($\sim 1 \times 10^7$) than for the Cu(II) porphyrins ($\sim 5 \times 10^5$) because of greater flexibility and larger g anisotropy of the $Cu(hfac)_2$ adducts than of the porphyrins. For the low-spin Fe(III) metmyoglobins A_{Ram} increases in the order $FeTPP(Im)_2^+$ (1.2×10^7) < R-Mb-Im (1×10^8) < R-Mb-CN (9×10^8), which parallels the order of increasing g anisotropy (Table 1).

Direct process. The weak temperature dependence that is characteristic of the direct process was observed for VOTTP-COOH, VOTTP-bipy, $CrO(HEBA)_2^-$, CrNTTP, $Cu(dtc)_2$, and CuTTP at low temperatures (Table 1). The data for tempone in sucrose octaacetate at temperatures below 77 K (Fig. 1) were obtained on a 0.7 mM sample. For a 2 mM sample the relaxation rates at temperatures below about 15 K were faster than for the lower concentration sample and that data could be fitted with a contribution from the direct process. In addition, we have observed that if samples are dissolved in solvents that crystallize (instead of forming a glass) the resulting locally high concentration of solute can result in a weak temperature dependence of $1/T_1$ similar to that predicted by the direct process. The relaxation that is observed under these conditions may be due to intermolecular electron–electron spin–spin interaction. Thus, the observation of a weak temperature dependence of $1/T_1$ at low temperatures may not always be due to the direct process for isolated spins. The samples used for the present study were prepared at relatively low concentrations (~millimolar) in glass-forming solvents to minimize intermolecular interactions. Saturation recovery measurements indicate that the concentrations used in these studies are low enough that relaxation rates for the samples reported here are not significantly concentration dependent at ~100 K. However, further tests of the concentration dependence of relaxation rates at temperatures below about 10 K will be required to distinguish between inter- and intramolecular contributions to the process that we refer to as the direct process in this report.

Local modes. For most of the transition metal complexes an additional process with a characteristic energy in the range of 185 to 350 K (130 to 240 cm^{-1}) was required to fit the data. These processes are tentatively assigned to local modes. Vibrations in this energy range have been observed for metalloporphyrins by resonance Raman spectroscopy (*52*). The coefficients, A_{loc}, were of the order of 10^5 for the $3d$ transition metals and increased to 4×10^6 and 1×10^7 for 4d Mo(V) and Ag(II), respectively. The increase in A_{loc} with increasing principal quantum number is consistent with increasing spin–orbit coupling for heavier transition metals. Because of the large values of A_{loc} the local mode contributions dominate over the Raman process for the complexes of Mo(V) and Ag(II). Further work is needed to determine whether this is a general phenomenon for complexes of heavier transition metals. The temperature dependence of g values for d^9 $[Ni(CN)_4Cl_2]^{5-}$ in NaCl has been assigned to low-frequency local anharmonic vibrations (*53*). The temperature dependence of the Raman spectrum of tetramethylbenzene has been assigned to a torsional mode at 190 cm^{-1} (*54*).

In an NMRD study of the relaxation of Cu(II)-substituted transferrin and native (copper–zinc) superoxide dismutase it was observed that the spin–lattice relaxation rate for the Cu(II) did not depend on the rotational correlation time for the protein (*55*). It was proposed that the relaxation occurred via vibrations of the protein that provided a "microcrystal" environment for the paramagnetic center (*55*). This observation suggests that the temperature dependence of relaxation rates observed for metal ions in proteins in rigid lattice may extrapolate into the slow tumbling region in fluid solution.

Thermally activated process. For several of the samples an additional contribution was observed at the highest temperatures for which data were available. This contribution was treated as a thermally activated process, although a comparable fit to the data could be obtained assuming another local mode with a characteristic energy approximately equal to the value of E_a used for the thermal process. To distinguish among a local mode, a thermally activated process, and an Orbach process requires experimental data at temperatures up to or beyond the temperature equivalent to the characteristic energy. It was possible to make this distinction only for the C_{60} anions. In this case the leveling off of the relaxation rates at high temperature is characteristic of a thermally activated process. Either an Orbach process or a local mode would predict that the relaxation rate would continue to increase with increasing temperature. Thus, the high temperature process for the C_{60} anions is assigned as thermal with an activation energy in the range of 330 to 370 K (230 to 255 cm^{-1}). The similarity in the activation energies for this thermal process for the different anions and different solvents and the observation that melting of the

solvent does not cause a discontinuity in the temperature dependence suggest that the dynamic process is a vibrational mode of the buckyball. The activation energy of 330 to 370 K (228 to 255 cm^{-1}) is within experimental uncertainty of the 271 cm^{-1} vibration observed for C_{60} and its anions (*56*).

Low-spin hemes. The experimental data for the low-spin hemes (Fig. 5 and Table 1) do not extend to high enough temperature to distinguish between an Orbach, local mode, or thermally activated process. Comparable fit to the available data can be obtained for each of these options with a characteristic energy of 240 to 275 K (165 to 190 cm^{-1}) (Table 1) that is approximately the same for the three systems examined. If the process is Orbach then the characteristic energy, Δ_{Orb}, would be the energy separation between the ground state and a low-lying electronic excited state. EPR *g*-values for low-spin Fe(III) can be analyzed to determine the energy of the low-lying excited state (*57*, *58*) in units of λ, the spin–orbit coupling constant. Application of this approach to $FeTPP(Im)_2^+$, R-Mb-Im, and R-Mb-CN gives energies of 2.23 λ, 1.68 λ, and 0.9 λ, respectively. Since it is likely that λ is similar for the three low-spin hemes, these calculations indicate that the energies for the low-lying electronic states are quite different for the three systems, which is not consistent with assignment of the process as Orbach with an approximately constant value of Δ_{Orb}.

Based on literature values of λ one can also estimate the energy of the low-lying excited state. The free ion value of λ for Fe(III) is about 500 cm^{-1} (*59*, *60*) and is expected to be smaller in complexes due to covalency. Levin and Brill obtained $\lambda = 350$ cm^{-1} for high-spin metmyoglobin (*61*). Baker and Figgis obtained values of λ between 260 and 270 cm^{-1} from EPR and magnetic susceptibility studies on low-spin Fe(III) complexes: tris(*o*-phenanthroline) iron(III), tris(2,2′-bipyridyl) iron(III), and hexacyanoferrate (*62*). Using these values as estimates of λ, the energy separations of 2.23 λ, 1.68 λ, and 0.9 λ correspond to 780 or 590 cm^{-1} for $FeTPP(Im)_2^+$, 588 or 445 cm^{-1} for R-Mb-Im, and 315 or 240 cm^{-1} for R-Mb-CN. These values are in the same range as the estimate of 355 to 590 cm^{-1} for the thermally accessible excited state of low-spin Fe(III) in horse heart ferrocytochrome *c* (*63*). The estimates for the energy of the low-lying excited state are substantially larger than the value of Δ_{Orb} that would be obtained if the high-temperature spin–lattice relaxation process were assigned as Orbach (165 to 185 cm^{-1}). This reasoning also suggests that assignment of the high-temperature process to an Orbach process involving a low-lying electronic excited state is not plausible.

Assignment to a local mode would require a vibrational frequency of 165 to 185 cm^{-1}. Resonance Raman spectra of heme proteins indicate that the Fe–N stretching frequency for the bond to the distal histidine is typically about 200 cm^{-1} (*64*). Thus, assignment of the high-temperature process to a local vibrational mode may be plausible. At room temperature, rotation around the Fe–N bond to coordinated imidazole is a relatively facile process in model Fe(III) porphyrinates (*65*), which suggests that low-amplitude oscillations might occur with a relatively low barrier even at lower temperatures. This process is another possibility for a thermally activated relaxation process. Comparison with results for other low-spin heme systems will be needed to test the plausibility of these proposals.

ACKNOWLEDGMENTS

The support of this work by National Institutes of Health Grants GM21156 (GRE and SSE) and GM57635 (BEB) is gratefully acknowledged. The sample of Nycomed symmetrical-trityl radical was a gift from Professor Howard Halpern (University of Chicago) and was provided to him by Nycomed Innovation AB.

REFERENCES

1. M. H. Rakowsky, A. Zecevic, G. R. Eaton, and S. S. Eaton, *J. Magn. Reson.* **131,** 97–110 (1998).
2. M. Seiter, V. Budker, J.-L. Du, G. R. Eaton, and S. S. Eaton, *Inorg. Chim. Acta* **273,** 354–366 (1998).
3. K. J. Standley and R. A. Vaughan, "Electron Spin Relaxation Phenomena in Solids," Plenum Press, New York (1969).
4. M. K. Bowman and L. Kevan, *in* "Time Doman Electron Spin Resonance" (L. Kevan and R. N. Schwartz, Eds.), pp. 68–105, Wiley-Interscience, New York (1979).
5. J. G. Castle, Jr. and D. W. Feldman, *Phys. Rev. A* **137,** 671–673 (1965).
6. J. G. Castle, Jr. and D. W. Feldman, *J. Appl. Phys.* **36,** 124–128 (1965).
7. D. W. Feldman, J. G. Castle, Jr., and G. R. Wagner, *Phys. Rev.* **145,** 237–240 (1966).
8. S. K. Hoffmann, W. Hilczer, and J. Goslar, *J. Magn. Reson. A* **122,** 37–41 (1996).
9. J.-P. Gayda, P. Bertrand, A. Deville, C. More, G. Roger, J. F. Gibson, and R. Cammack, *Biochim. Biophys. Acta* **581,** 15–26 (1979).
10. P. Bertrand, J.-P. Gayda, and K. K. Rao, *J. Chem. Phys.* **76,** 4715–4719 (1982).
11. V. I. Muromtsev, N. Ya. Shteinshneider, S. N. Safranov, V. P. Golikov, A. I. Kuznetsov, and G. M. Zhidomirov, *Fiz. Tverd. Tela* **17,** 813 (1975) (p. 517–519 in transl.).
12. J.-L. Du, S. S. Eaton, and G. R. Eaton, *J. Magn. Reson. A* **115,** 213–221 (1995).
13. J.-L. Du, G. R. Eaton, and S. S. Eaton, *J. Magn. Reson. A* **115,** 236–240 (1995).
14. R. Husted, J.-L. Du, G. R. Eaton, and S. S. Eaton, *Magn. Reson. Chem.* **33,** S66–S69 (1995).
15. J.-L. Du, G. R. Eaton, and S. S. Eaton, *J. Magn. Reson A* **117,** 67–72 (1995).
16. J.-L. Du, G. R. Eaton, and S. S. Eaton, *J. Magn. Reson. A* **119,** 240–246 (1996).
17. S. Andersson, F. Radner, A. Rydbeek, R. Servin, and L.-G. Wistrand, Nycomed Imaging AS, U.S. Patent 5,530,140.
18. J. H. Ardenkjaer-Larsen, I. Laursen, I. Leunbach, G. Ehnholm, L.-G. Wistrand, J. S. Petersson, and K. Golman, *J. Magn. Reson.* **133,** 1–12 (1998).

19. Y. Zhou, B. E. Bowler, G. R. Eaton, and S. S. Eaton, to be published.
20. B. A. Springer and S. G. Sliger, *Proc. Natl. Acad. Sci. USA* **84,** 8961–8965 (1987).
21. G. N. Phillips, Jr., R. M. Anduini, B. A. Springer, and S. G. Sliger, *Proteins: Struct. Funct. Genet.* **7,** 358–365 (1990).
22. K. Nakagawa, M. B. Candelaria, W. W. C. Chik, S. S. Eaton, and G. R. Eaton, *J. Magn. Reson.* **98,** 81–91 (1992).
23. S. S. Eaton, A. Kee, R. Konda, G. R. Eaton, P. C. Trulove, and R. T. Carlin, *J. Phys. Chem.* **100,** 6910–1619 (1996).
24. J. M. Burchfield, J.-L. Du, K. M. More, S. S. Eaton, and G. R. Eaton, *Inorg. Chim. Acta* **263,** 23–33 (1997).
25. G. R. Eaton and S. S. Eaton, *J. Magn. Reson.* **136,** 63–68 (1999).
26. R. Konda, J.-L. Du, S. S. Eaton, and G. R. Eaton, *Appl. Magn. Reson.* **7,** 185–193 (1994).
27. M. H. Rakowsky, K. M. More, A. V. Kulikov, G. R. Eaton, and S. S. Eaton, *J. Am. Chem. Soc.* **117,** 2049–2057 (1995).
28. R. W. Quine, S. S. Eaton, and G. R. Eaton, *Rev. Sci. Instrum.* **63,** 4252–4262 (1992).
29. A. Abragam, "The Principles of Nuclear Magnetism," Oxford Univ. Press, London (1961), pp. 405–409.
30. J. Murphy, *Phys. Rev.* **145,** 241–247 (1966).
31. R. Orbach, R. *Proc. Phys. Soc. (Lond.)* **77,** 821–826 (1961).
32. V. A. Atsarkin, V. V. Demidov, and G. A. Vasneva, *Phys. Rev. B* **56,** 9448–9453 (1997).
33. M. R. Caira, J. M. Haigh, and L. R. Nasimbeni, *J. Inorg. Nucl Chem.* **34,** 3171–3176 (1972).
34. L. L. van Reijen, P. Cossee, and H. J. van Haren, *J. Chem. Phys.* **38,** 572–573 (1963).
35. J. P. Allen, J. T. Colvin, D. G. Stinson, C. P. Flynn, and H. J. Stapleton, *Biophys. J.* **38,** 299–310 (1982).
36. V. Budker, J.-L. Du, M. Seiter, G. R. Eaton, and S. S. Eaton, *Biophys. J.* **68,** 2531–2542 (1995).
37. A. H. Morrish, "The Physical Principles of Magnetism," Wiley, New York (1965), pp. 96–98.
38. D. L. Huber, *J. Non-Cryst. Solids* **51,** 241–244 (1982).
39. D. L. Huber, *J. Luminescence* **36,** 327–329 (1987).
40. E. Whalley and H. J. Labbe, *J. Chem. Phys.* **51,** 3120–3127 (1969).
41. H. Siethoff and K. Ahlborn, *Phys. Stat. Sol (b)* **190,** 179–191 (1995).
42. G. Nagendrappa, R. Somashekar, M. S. Madhava, and P. G. Ramappa, *Ind. J. Phys.* **70A,** 637–640 (1996).
43. P. I. Ktorides, D. L. Uhrich, R. M. D'Sidocky, and D. L. Fishel, *J. Chem. Phys.* **77,** 4188–4198 (1982).
44. R. Barbieri, A. Silvestri, L. Pellerito, A. Gennaro, M. Petrera, and N. Burriesci, *J. Chem. Soc. Dalton Trans.* 1983–1987 (1980).
45. Y. Q. Jia, H. Z. Liang, Q. Shen, M. Z. Jin, M. L. Liu, and X. W. Liu, *Phys. Stat. Sol. A* **147,** 249–254 (1995).
46. A. G. Staib and M. C. Boehm, *J. Chem. Phys.* **91,** 4961–4973 (1989).
47. M. K. Bowman and L. Kevan, *Faraday Discuss. Chem. Soc.* **63,** 7–17 (1977).
48. D. Kovala-Demertzi, P. Tauridou, A. Moukarika, J. M. Tsangaris, C. P. Raptopoulou, and A. Terzis, *J. Chem. Soc. Dalton Trans.* 123–128 (1995).
49. G. Wortmann, E. A. Bychkov, and Yu. S. Grushko, *Hyperfine Inter.* **70,** 1179–1184 (1992).
50. M. Z. Jin, M. L. Liu, X. W. Liu, Y. T. Jin, and Y. Q Jia, *Phys. Stat. Sol. A* **133,** 333–339 (1992).
51. R. Barbieri, G. Ruisi, A. Silvestri, A. M. Giuliani, A. Barbieri, G. Spina, F. Pieralli, and F. D. Giallo, *J. C. S. Dalton Trans.* 467–475 (1995).
52. T. G. Spiro, in "Iron Porphyrins," Part II (A. B. P. Lever and H. B. Gray, Eds.), Addison-Wesley, Reading, MA (1983), pp. 89–159.
53. N. V. Vugman and M. R. Amaral, Jr., *Phys. Rev. B* **42,** 9837–9842 (1990).
54. C. B. Harris, R. M. Shelby, and P. A. Cornelius, *Phys. Rev. Lett.* **38,** 1415–1419 (1977).
55. I. Bertini, C. Luchinat, R. D. Brown, III, and S. H. Koenig, *J. Am. Chem. Soc.* **111,** 3532–3536 (1989).
56. F. Negri, G. Orlandi, and F. Zerbetto, *Mol. Cryst. Liq. Cryst* **234,** 155–160 (1993).
57. G. Palmer, *in* "The Porphyrins," Vol. IV (D. Dolphin, Ed.), Chapter 6, pp. 313–353, Academic Press, New York (1979).
58. G. Palmer, *in* "Iron Porphyrins," Part II (A. B. P. Lever and H. B. Gray, Eds.), Chapter 2, pp. 43–88, Addison-Wesley, Reading, MA (1983).
59. A. Abragam and B. Bleaney, "Electron Paramagnetic Resonance of Transition Ions," Oxford Univ. Press, London (1970), p. 391.
60. J. R. Pilbrow, "Transition Ion Electron Paramagnetic Resonance," Oxford Univ. Press, Oxford (1990), p. 144.
61. P. D. Levin and A. S. Brill, *J. Phys. Chem.* **92,** 5103–5110 (1988).
62. J. Baker and B. N. Figgis, *J. Chem. Soc.,* 598–602 (1975).
63. L. Banci, I. Bertini, C. Luchinat, R. Pierattelli, N. Shokhirev, and F. A. Walker, *J. Am. Chem. Soc.* **120,** 8472–8479 (1998).
64. T. G. Spiro, *in* "Iron Porphyrins," Part II (A. B. P. Lever and H. B. Gray, Ed.), pp. 89–159, especially p. 109. Addison-Wesley, Reading, MA (1983).
65. K. I. Momot and F. A. Walker, *J. Phys. Chem. A* **101,** 2787–2795 (1997).